Received: 30 October 2021 | Revised: 13 July 2022 | Accepted: 16 July 2022

DOI: 10.1002/joc.7810

RESEARCH ARTICLE

International Journal of Climatology RMetS

Sensitivity of seasonal air temperature and precipitation, and onset of snowmelt, to Arctic Dipole modes across the Taiga Plains, Northwest Territories, Canada

Bhaleka D. Persaud[1] | **Laura E. Chasmer**[2] | **William L. Quinton**[1] | **Brent B. Wolfe**[1] | **Michael C. English**[1]

[1]Department of Geography and Environmental Studies, Wilfrid Laurier University, Waterloo, Ontario, Canada

[2]Department of Geography and Environment, University of Lethbridge, Lethbridge, Alberta, Canada

Correspondence
Bhaleka D. Persaud, Department of Geography and Environmental Studies, Wilfrid Laurier University, Waterloo, ON N2L 3C5, Canada.
Email: pers3479@mylaurier.ca

Funding information
ArcticNet; Wilfrid Laurier University; Canada First Research Excellence Fund

Abstract

Northern high latitudes are experiencing some of the greatest increases in air temperatures on Earth. Air temperatures (along with other modulating variables including precipitation and the onset of snowmelt) are influenced by atmospheric–oceanic circulation patterns, some of which are persistent and recurrent. One pattern in particular, the Arctic Dipole (AD) anomaly, is a persistent sea-level pressure teleconnection pattern between the Canadian Archipelago and Barents Sea that has unknown impacts on local climate variability. These patterns may be important, especially in hydro-ecologically sensitive areas such as Northwest Territories (NWT), Canada where permafrost thaw and ecosystem changes are influenced by interannual climate variability. The goal of this research is to determine the impacts of the AD on local climate (air temperature, precipitation, snowmelt) for a 66-year period (1950–2015) spanning both latitudinal and longitudinal gradients across NWT from north to south and foothills to plains. Deviations during strong positive and negative modes of the AD index were calculated in reference to the complete 66-year record. Results showed considerable year-to-year variability in the AD pattern, with more frequent strong negative modes during the 2000s. During 1950–2015, there were 64 and 56 occurrences of strong positive and strong negative AD modes, respectively, across all seasons. Spring and summer strong AD modes led to local air temperature anomalies of greater than 0.8°C compared with the long-term (66 years) mean. Earlier onset of snowmelt, by an average of 3–5 days, was also noted during positive AD modes. Despite strong connectivity between the AD and local air temperature, we found less correspondence between the AD and seasonal precipitation. These findings improve understanding of the impacts of the AD on local weather and climate in NWT and suggest implications for ecosystem change, such as drying and shrubification of northern boreal peatlands and possible connectivity to teleconnection impacts on wildland fire.

KEYWORDS

Arctic Dipole anomaly, geopotential heights, high latitude, snowmelt, surface climate, teleconnection

1 | INTRODUCTION

Global air temperatures have increased during the past century and are predicted to increase in the coming decades (IPCC, 2021). High-latitude regions have been especially prone to both increases and greater range of variability in air temperatures (IPCC, 2021). The surface climate of northern Canada is largely influenced by synoptic scale atmospheric circulation patterns. The strength and location of mid-tropospheric troughs and ridges drive the movement and persistence of air masses across the region (Klock *et al*., 2001; Newton *et al*., 2014). For example, rapid warming in northern Canada, resulting in earlier snowmelt in spring and later onset of snow in autumn, impacts permafrost thaw and ecosystem change (e.g., Chasmer and Hopkinson, 2017; Connon *et al*., 2021). These observations have also led to increased interest in atmospheric circulation patterns and the influences that these may have on inter- and intra-annual climate variability. Climate anomalies can have numerous implications, including ecosystem threshold responses, changing hydrological processes, and ecosystem services (Newton *et al*., 2014; Vincent *et al*., 2015; Chasmer and Hopkinson, 2017; Tan *et al*., 2019). The combined effects of atmospheric circulations and climate change in northern Canada are not well-understood, thereby creating uncertainties in our understanding of the long-term impacts of these changes on ecosystems, water resources, and northern communities (Woo *et al*., 2008; Serreze and Barry, 2014; Shi *et al*., 2015; Vincent *et al*., 2015; DeBeer *et al*., 2016).

Variations in air temperature are driven by global atmospheric circulation, modified by recurrent and persistent atmospheric–oceanic patterns (specifically sea surface temperature–atmosphere relationships), referred to as teleconnection patterns (Wallace and Gutzler, 1981; Barnston and Livezey, 1987). Teleconnection patterns are recognized for their opposing centre of action (dipole) of atmospheric pressures and/or sea surface air temperature anomalies, with dipoles typically located between 2,000 and 6,000 km apart. As such, these patterns influence weather and climate across various temporal and spatial scales, which are driven, in part, by phase (positive or negative) and strength. The phase and strength of the patterns vary temporally and can impact air temperature and precipitation to greater or lesser amounts, depending on location (Jiang *et al*., 2014; Vincent *et al*., 2015). The influence and magnitude of the opposing dipole systems are typically described using a teleconnection index (Barnston and Livezey, 1987).

The Arctic Oscillation (AO) is one of the dominant atmospheric circulation modes in the Northern Hemisphere and is characterized by a north–south dipole structure of the sea level pressure (SLP) pattern with one sign in the Arctic and the opposite sign at ~45° latitude (Thompson and Wallace, 1998). The positive mode of the AO index has lower SLP anomalies in the Arctic and higher SLP anomalies in the Northern Hemisphere mid-latitudes, resulting in strengthened westerlies, northward shift in the jet stream, and fewer periods of cold air outbreaks, while during the negative mode in the AO, the opposite occurs (Thompson and Wallace, 1998). Previous studies also explored the relationship between the AO and Canada's weather and climate across various temporal and spatial scales (Déry and Wood, 2004; Fleming *et al*., 2006; Déry *et al*., 2009; Bonsal and Shabbar, 2011; Tan *et al*., 2019). Positive AO index was associated with consistently higher spring and summer air temperatures in southwestern Yukon and northwestern British Columbia (Fleming *et al*., 2006), while Déry and Wood (2004) noted that between 1964 and 2000, positive AO index was associated with cooler and drier conditions over northern Canada. While the impacts of the AO are known, there may be other northern teleconnection patterns that also influence climate variability in northern high latitudes (Déry *et al*., 2009).

Another, lesser-known teleconnection pattern in the Arctic is the Arctic Dipole (AD) (Wu *et al*., 2005; Watanabe *et al*., 2006; Wang *et al*., 2009; Overland *et al*., 2012). The AD pattern is associated with a SLP dipole between the Canadian Archipelago and northern Siberia/Barents Sea (Wang *et al*., 2009; Overland *et al*., 2012). Overland *et al*. (2012) stated when there are positive SLP anomalies in the Canadian Archipelago/Beaufort Sea and negative SLP anomalies in the northern Siberia/Barents Sea (negative AD), a strong meridional wind is observed from the western to eastern Arctic. This wind pattern has led to the movement of sea ice out of the Arctic and into the northern Atlantic Ocean via the Trans-Polar Drift Stream, resulting in warming of the Arctic (Wang *et al*., 2009; Overland *et al*., 2012). This SLP anomaly strengthens local southerly winds and promotes northward movement of warm water in the Pacific Ocean, resulting in increased oceanic heat flux into the Arctic Ocean via the Bering Strait (Wang *et al*., 2009; Overland *et al*., 2012). This impacts sea ice by accelerating melt and amplifying ice–albedo feedback (Wang *et al*., 2009; Lei *et al*., 2016; Heo *et al*., 2021). Overland *et al*. (2012) found that enhanced negative mode of the AD was coincident with dramatic ice loss in the Arctic Ocean beginning in 2007. The opposite occurs during the positive AD phase. The prominence of the AD as a driver of ice loss has raised questions pertaining to its influence on northern continental regions (Zhang *et al*., 2008; Wang *et al*., 2009; Tang *et al*., 2014; Choi *et al*., 2019; Xiao *et al*., 2020). These include the Northwest Territories (NWT) Canada, as sea

ice reduction can influence changes of local climate extending inland (Budikova, 2009).

The AD has also been linked to various weather patterns in many regions in the Northern Hemisphere (Wu *et al.*, 2009; Matsumura *et al.*, 2014; Cai *et al.*, 2018; Fazel-Rastgar, 2020; Horvath *et al.*, 2021). For instance, Cai *et al.* (2018) used European Centre for Medium-Range Weather Forecasts Reanalysis (ERA-Interim reanalysis) data and showed that for North America, higher SLP is associated with positive air temperature anomalies (greater than long-term average temperature) during summer months, while both negative and positive precipitation anomalies prevailed. Using 30 models from CMIP5 (Coupled Model Intercomparison Project Phase 5) to determine the impacts AD will have on climate from 2006 and 2100, Cai *et al.* (2018) predicted that atmospheric circulation patterns associated with the AD will have a larger impact on summer precipitation variability over the Arctic in the future. The heatwaves during summer 2007, 2012, and 2016 in the Canadian Arctic were also attributed to the AD (Fazel-Rastgar, 2020) indicating that severe weather anomalies may be associated with these patterns. There is also evidence to suggest that the dipole pattern has become more pronounced since the 2000s with stronger high and low SLP anomalies and high AD index values (Overland *et al.*, 2012). This has been linked to earlier spring snowmelt between 1988 and 2011 in Eurasia and associated with positive SLP anomaly over the Arctic and negative SLP anomaly over Eurasia (Matsumura *et al.*, 2014). Horvath *et al.* (2021) also found earlier melt onset during positive SLP dipole over the Arctic over a longer temporal period (1979–2018). In Canada, increasing temperature and decreasing snow cover indices are only partly explained by other teleconnections (Vincent *et al.*, 2015). These authors concluded that anthropogenic forces were responsible for most the observed changed in climate variables in Canada (Vincent *et al.*, 2015). However, these authors did not examine the influence of AD circulation on Canada's weather and climate.

Here, we examine the seasonal impacts of the AD oscillation on local weather across a latitudinal gradient of sites in the Taiga Plains ecozone, NWT, Canada from 1950 to 2015. The objectives of this study are to (a) quantify relationships between strong seasonal modes of the AD and coincident surface climate variables (air temperature, precipitation, and the onset of snowmelt); (b) explore physical mechanisms, including pressure dipoles associated with these relations, which could alter local weather; and (c) discuss the implications of these changes on terrestrial ecosystems in Taiga Plains. The findings presented provide greater understanding of the historical impacts of AD on surface climate variables and mechanisms responsible and provide a framework for more detailed investigations, which can lead to better models used in weather and climate forecasting across NWT communities.

2 | DATA AND METHODS

2.1 | Study area

The study sites are located between 60°–70°N latitude and 101°–130°W longitude, spanning the mainly the Taiga Plains, NWT (Figure 1). All sites include long-term meteorological records collected by Environment and Climate Change Canada and have been included in earlier regional research initiatives (e.g., the Mackenzie GEWEX study; Woo *et al.*, 2008). The Taiga Plains is Canada's sixth largest ecozone, with distinct ecological, climatic, and landscape features (Phillips, 1990). Drained by Canada's largest river, the Mackenzie, approximately 90% of the Taiga Plains, is located within the western NWT, with small extensions into northeastern British Columbia and northern Alberta. For this study, the Taiga Plains was subdivided into northern, foothills, lake, and southern regions based on geography, latitude, and proximity to mountains, lakes, and other landforms, which may be differentially affected by climate (Ecosystem Classification Group, 2009). The Taiga Plains is bounded to the east by the Taiga Shield including Great Slave Lake and Great Bear Lake, to the west by the foothills of the Mackenzie Mountains, to the north by the Mackenzie Delta, and to the south by a mix of black spruce dominated peatlands and upland mixedwood of the Boreal Plains (Ecosystem Classification Group, 2009).

The climate of the Taiga Plains includes long cold winters and short, cool summers (Phillips, 1990). Winters are characterized by the dominance of cold, dry high Arctic high-pressure systems. During spring, summer, and autumn, weak low-pressure systems originating in the Beaufort Sea and Gulf of Alaska bring moist air to the region. Occasionally, low-pressure systems originating from the Pacific Ocean generate substantial precipitation (Dyke and Brooks, 2000). Mean annual air temperature varies from −10.1 to −2.6°C, while mean annual precipitation ranges from 160 to 388 mm (Ecosystem Classification Group, 2007), with highest cumulative precipitation occurring in the Cordillera and southern NWT (Phillips, 1990). Rainfall accounts for nearly half of precipitation (Phillips, 1990). Snowmelt typically commences in early April to mid-May (Dyke and Brooks, 2000).

2.2 | Arctic Dipole index

The AD index, derived by Overland *et al.* (2012), is the second leading principal component of the mean SLP

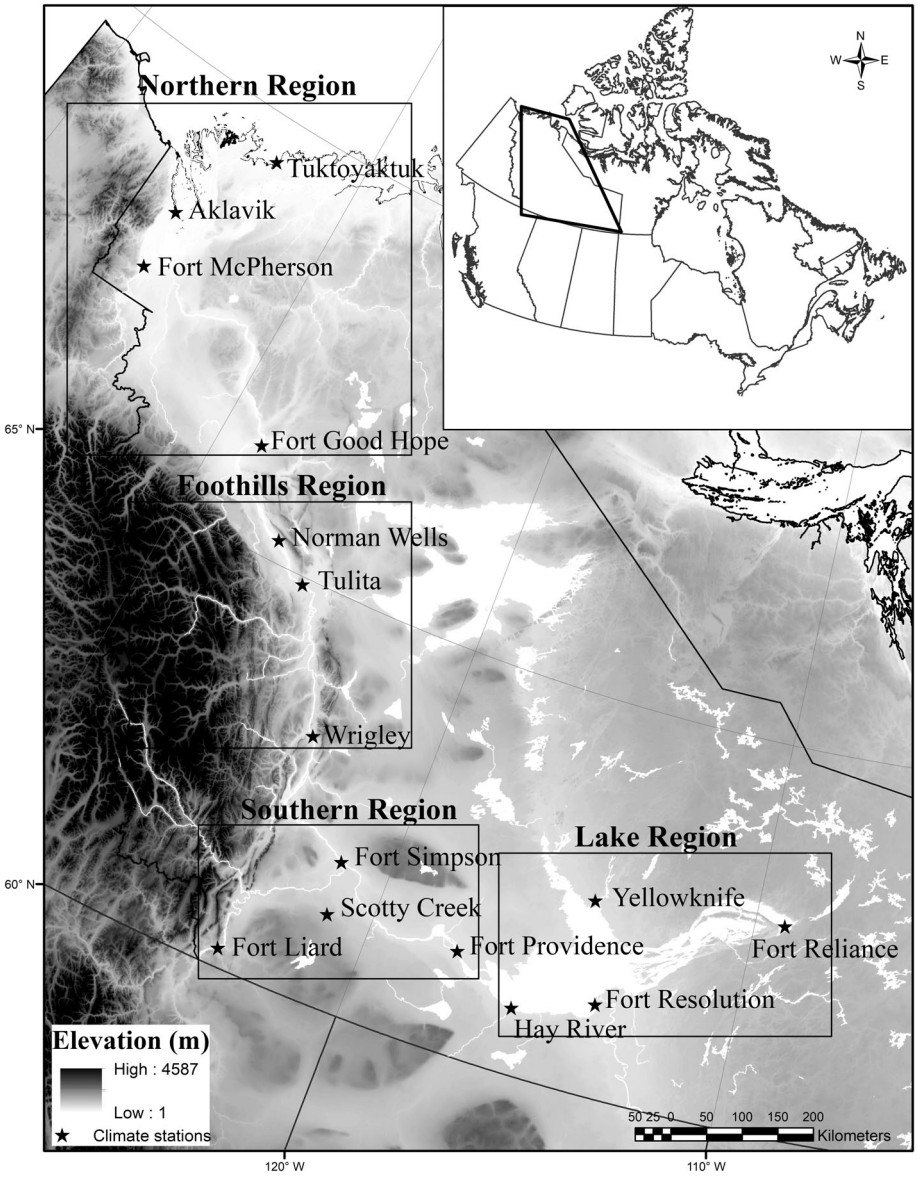

FIGURE 1 Locations of the study domain (inset map) and study sites (black stars)

north of 70°N. Although the literature agrees on the existence of the SLP dipole and calculation of the AD index (Wu *et al*., 2005; Wang *et al*., 2009; Overland *et al*., 2012), there are opposing definitions of negative and positive AD. Unless otherwise indicated, in this study, the negative (positive) AD mode circulation is defined as positive (negative) sea level pressure (SLP) anomalies in the Canadian Archipelago and negative (positive) SLP anomalies in the northern Siberia/Barents Sea (Figure 2) (Overland *et al*., 2012; Choi *et al*., 2019). The standardized AD index is defined for each season as the AD principal component index value per year subtracted from the 1950–2015 long-term mean divided by the standard deviation (Overland *et al*., 2012). The seasonal standardized AD index from 1950 to 2015 was downloaded from the NOAA Bering Climate website (NOAA, 2021). Meteorological seasons were defined as winter (December–February), spring (March–May), summer (June–August), and autumn (September–November). To the best of the authors' knowledge, there is no consensus on the quantitative strength thresholds for AD classifications. For this study, standardized AD index (herein refer to AD index) values exceeding ±0.5 were classified as strong positive or strong negative modes, following methods applied to other teleconnection pattern classifications (Trenberth, 1997).

2.3 | Climate data

Daily interpolated air temperature and precipitation data were obtained from National Resources Canada (Hutchinson *et al*., 2009; NRCAN, 2019). These air temperature and precipitation data were interpolated using

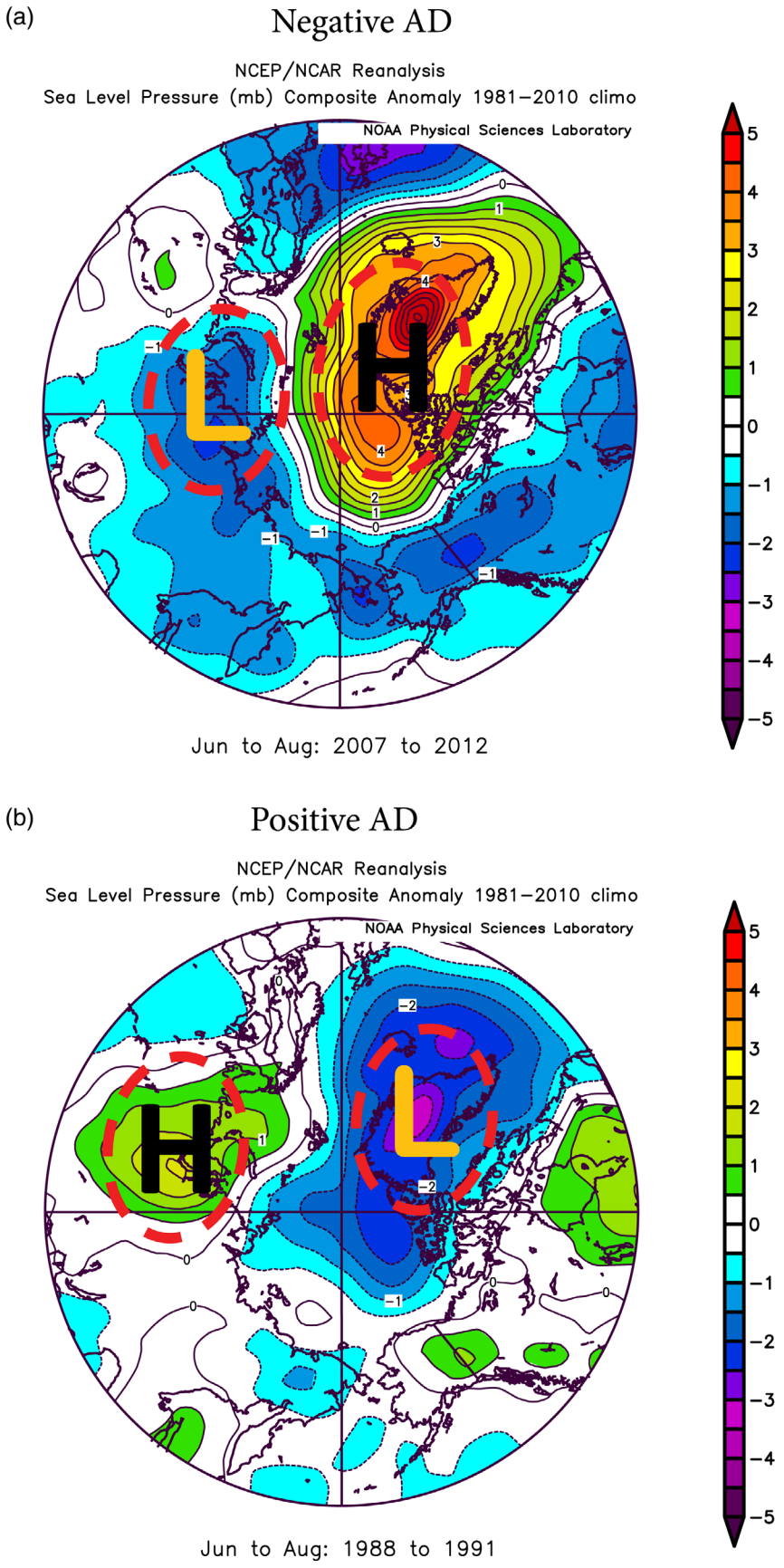

FIGURE 2 Example multiyear composite sea level pressure (SLP) anomaly patterns, that is SLP deviation from long-term averages, in summer (June–July–August), during (a) the strong negative AD mode from 2007 to 2012, and (b) the strong positive AD mode from 1988 to 1991. Data are from the NCEP–NCAR Reanalysis through the NOAA/Earth Systems Research Laboratory (NOAA, 2020) [Colour figure can be viewed at wileyonlinelibrary.com]

Australian National University Spline (ANUSPLIN), using a thin plate smoothing spline methodology (Hutchinson *et al*., 2009; McKenney *et al*., 2011) and applied by National Resources Canada at a cell resolution of approximately 10 km^2 from 1950 to 2015 (McKenney *et al*., 2011). Interpolated data from ANUSPLIN have been used as an alternative to in situ data in areas where data consistency may be limited and gaps in data collection may occur and uncertainty over northern regions is high due to the low spatial coverage of in situ climate stations. Exploring of teleconnection impacts, such as AD and AO, on northern Canada's climate has received little attention because there are very few in situ stations with long-term consistent records. However, evaluation of ANUSPLIN interpolated data has low bias compared with in situ observation data across northwestern Canada (Wong *et al*., 2017; Persaud *et al*., 2020).

Daily air temperature and precipitation data were obtained from nearest interpolated cells at each location (Figure 1). Average air temperatures were aggregated for each season from interpolated daily maximum and minimum air temperature. Seasonal air temperature and precipitation anomalies for each site were computed as the difference between the annual seasonal value and the 66-year (1950–2015) average. A positive anomaly indicates that the observed air temperature (precipitation) was warmer (wetter) than the long-term seasonal average, while a negative anomaly indicates that the observed temperature (precipitation) was cooler (drier) than the long-term average. The date of sustained snowmelt was defined as the first day in which the mean daily air temperature was higher than 0°C following the final consecutive 5-day period between March and May when the daily mean air temperature was less than 0°C (Shi *et al*., 2015). Air temperature and precipitation anomalies and onset date of snowmelt were compared to the positive and negative modes of the AD.

To explore mechanistic understanding between air temperature, snowmelt onset, and precipitation, and positive and negative modes of the AD, this study adapted an approach utilized by Overland *et al*. (2012). Geopotential height from National Centres for Environmental Prediction/National Centre for Atmospheric Research (NCEP/NCAR) reanalysis data (Kalnay *et al*., 1996) were accessed and visualized using the NOAA Climate Analysis and Plotting tool (NOAA, 2020). Geopotential heights at 850–500 mb were selected for this exploratory analysis because they are relatively free from atmospheric boundary layer influences, while describing upper-level tropospheric patterns (Francis and Vavrus, 2015). To provide insights on the implications of the AD on NWT terrestrial ecosystem climate, this study incorporated findings from the literature.

2.4 | Statistical analysis

All statistical analyses were undertaken using R 3.5.3 Project software (R Development Core and Team, 2016). The nonparametric Kruskal–Wallis test *kruskal.test* function in R was used to evaluate relationships among climate variables (air temperature, precipitation, and onset of snowmelt) and the two AD modes at each site. Here, the null hypothesis states that there was no difference among climate variables during the two modes (strong positive and strong negative) of the AD at sites. Nonparametric tests were chosen because climate variables often demonstrated a skewed distribution (Helsel and Hirsch, 1992). Additionally, Tukey honest significant differences (HSD) post hoc tests were used to assess the statistical significance of differences among site means during positive and negative AD modes. Post hoc analysis provides insight into the similarities/differences between specific groups and is, therefore, an essential step in data analysis (Tukey, 1949). In all cases, differences were considered statistically significant when $p < .05$.

3 | RESULTS

3.1 | Temporal distribution of the seasonal Arctic Dipole index

The AD index displays considerable annual variability in magnitude with few clear temporal trends from 1950 to 2015 (Figure 3). Some years and seasons exhibit periods of strong positive (AD $\geq$ 0.5) modes and others display strong negative AD modes (AD $\leq$ −0.5). The AD index varied from −1.75 (summer 1958) to 1.28 (summer 1994), illustrating the range of variability during the past 66 years. Analysis of the AD index time series data for all seasons indicate a total of 64 (24%) and 56 (21%) occurrences were in the strong positive and strong negative AD modes, respectively. In winter, mostly strong positive values occurred from 1953 to early 1957 (0.59–1.01), and strong negative AD index (ranged from −0.54 to −1.01) between 1958 and 1977 (Figure 3a). Between 1990 and the early 2000s, AD index values remained negative but were also of smaller magnitude (from −0.24 to −0.54). There has not been another strong negative AD mode in winter since 2004. The spring AD index is largely characterized by frequent strong positive modes (from 0.55 to 1.21) occurring during the early 1970s to 1995 (Figure 3b). This was followed by a period (late 1990s to mid-2000s) of consistently strong negative AD values, ranging from −0.55 to −1.04. During summer between mid-1965 and 2000, the AD index was characterized by

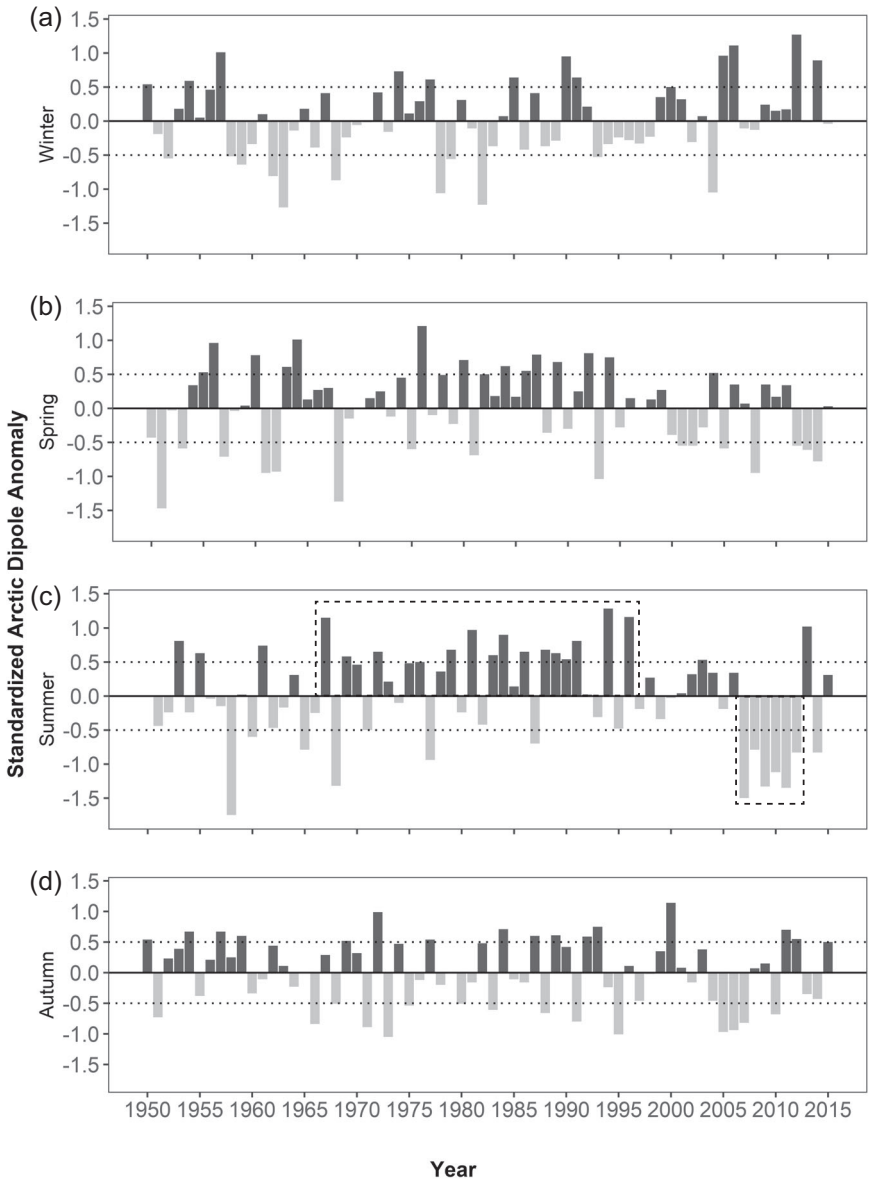

FIGURE 3 Standardized AD for (a) winter, (b) spring, (c) summer, and (d) autumn. Grey bars are negative AD anomalies and black bars are positive AD anomalies. Indices exceeding ±0.5 threshold (dashed lines) are defined as strong ±AD modes. The dashed black boxes highlight areas mentioned in the text

mostly positive values, with strong positive values (from 0.63 to 0.81) between 1988 and 1991 (Figure 3c). A noticeable feature in the summer AD index is the abrupt change to more persistent, and the strongest recorded, negative AD index between 2002 and 2007, which ranged from −0.79 to −1.5. The autumn AD index (Figure 3d) pattern is similar to summer during strong modes, but with reduced magnitude.

3.2 | Geopotential height patterns during periods of strong negative and positive AD mode

To explore mechanistic understanding of atmospheric circulation patterns during strong AD modes, variations in middle- to upper-level geopotential height patterns over the NWT during strong negative AD mode (2007–2012; Figure 4a,b) and positive AD mode (1988–1991; Figure 4c, d) were examined. When compared with the long-term average for 2007–2012 period, greater geopotential heights (ranges from 3,020 to 3,060 m) and therefore, greater geopotential anomalies (Figure 4b) were observed near southern and lake sites in the negative AD mode. In contrast, during the same period, the northern sites showed that the ridge had reduced amplitude, lower geopotential heights (ranges from 2,980 to 3,010 m) and lower geopotential height anomalies (Figure 4a). While in the positive AD summers of 1988–1991, there was a broad region of high geopotential heights prevalent over continental Canada combined with a mid-level ridge over NWT, whose axis appears more elongated and amplified northwards (over Alaska/Yukon and southern NWT; Figure 4b). The elongated high amplitude ridge observed

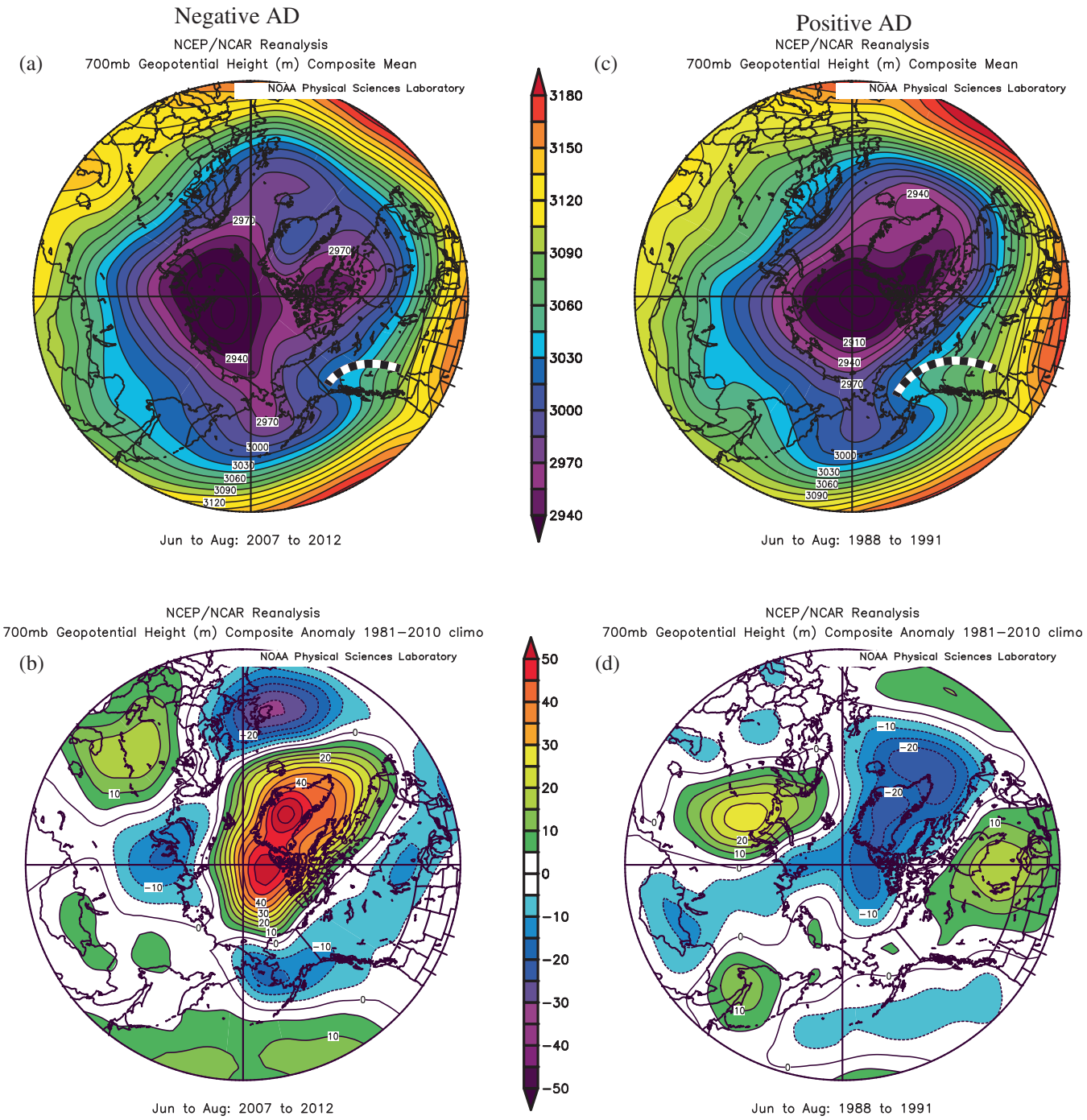

FIGURE 4 Summer multiyear composite during a strong negative AD mode 2007–2012 for the (a) 700 hPa geopotential height mean and (b) 700 hPa geopotential height anomaly and during a strong positive AD mode (1988–1991) (c) mean 700 hPa geopotential height and (d) 700 hPa geopotential height anomaly. Data and plotting tool used for data are from the NCEP–NCAR Reanalysis through the NOAA/Earth Systems Research Laboratory (NOAA, 2020). Dashed black and white lines on figures represent the ridge axis [Colour figure can be viewed at wileyonlinelibrary.com]

during summer positive AD (Figure 4b) suggests advection of stronger southwesterly warm air masses (Overland *et al.*, 2012) towards NWT from the warmer Pacific Ocean, potentially contributing to positive air temperature anomalies. A similar anomaly pattern, with reduced variability, existed from 850 to 500 hPa geopotential height fields (not shown) during these two same periods.

3.3 | Positive and negative modes of the AD index and air temperature

The seasonal distribution of air temperature anomalies in strong positive and negative AD modes showed some consistent patterns across a latitudinal gradient in the NWT, illustrated in Figure 5. Air temperature anomalies

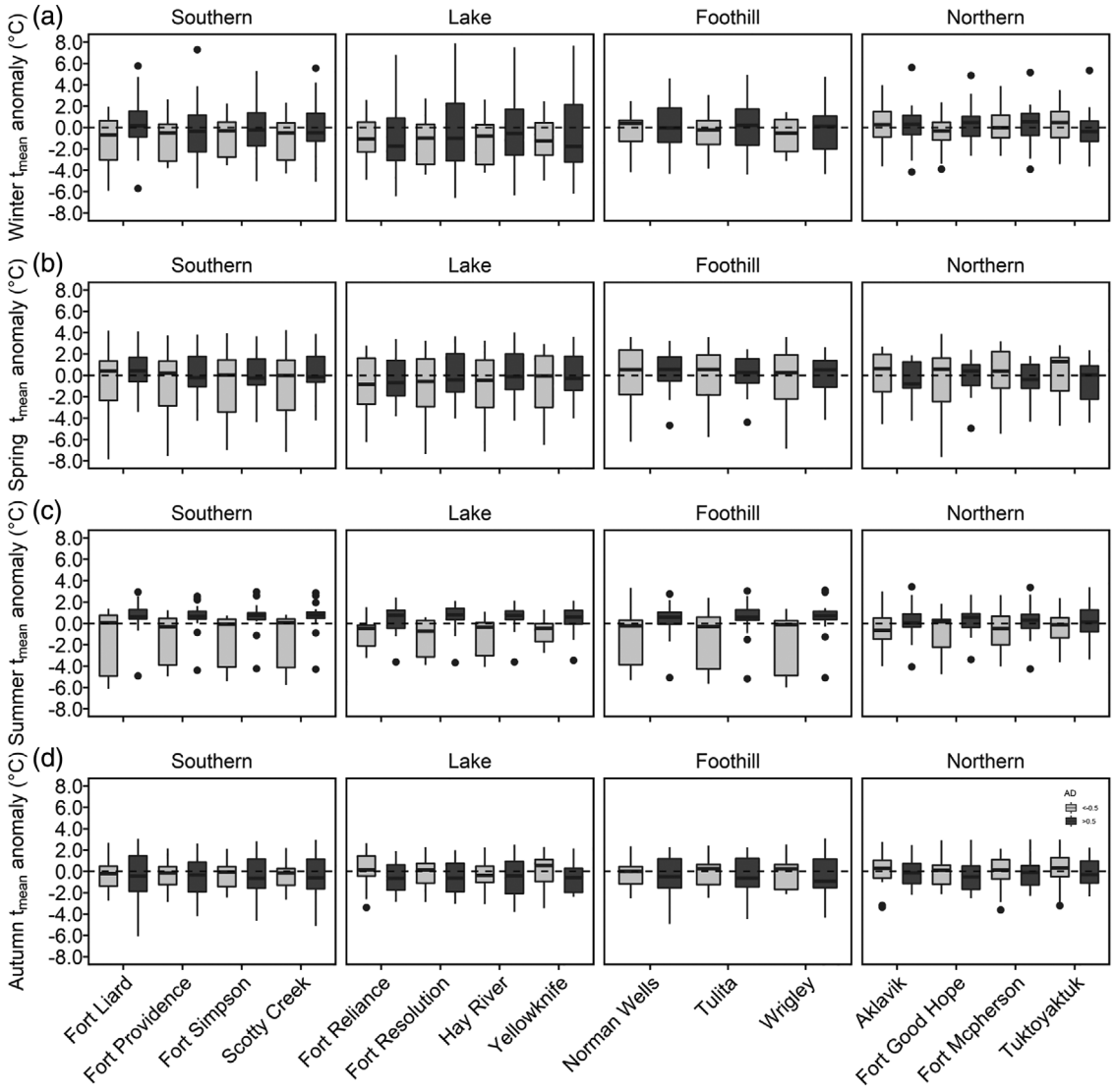

FIGURE 5 Boxplots showing the distribution of winter, spring, summer, and fall AD modes exceeding the ±0.5 threshold and its corresponding mean temperature anomaly. Black boxes represent positive AD mode while grey boxes represent negative AD mode, while black dots represent outliers

correspond with strong positive and negative mode AD anomalies across 73% of sites ($p < .05$; Figure 5 and Table 1). Air temperature anomalies vary less in winter [standard deviation (σ) ranges from 1.8 to 3.1°C] compared with air temperature anomalies in other seasons. Further, these shift towards cooler temperature anomalies (between −0.9 and −2.5°C) during both modes of the AD. In spring, air temperature anomalies show an emerging response to AD modes (Figure 5b). During strongly positive AD mode, the standard deviation (σ) of the spring air temperature anomaly is low, with σ ranging from 1.8 to 2.2°C, while during strong negative AD mode the σ spring air temperature anomaly increases (σ = 2.5–3.3°C), illustrating greater magnitude, especially in southern, lake, and foothill regions (Figure 1). Similar AD–air temperature patterns were observed in summer for both modes (Figure 5c and Table 1). During positive AD modes, significantly greater median summer air temperature anomalies were observed ($p < .05$): southern (1.1°C), lake (1.1°C), and foothill (1.0°C) regions. Similarly, there was also an observed decrease in standard deviation ($\sigma = \sim 1.5$°C) of air temperature anomalies across all regions. During the negative AD mode, increased variance in the range of temperatures occurred across all regions (Figure 5c and Table 1). During the negative AD mode, greater variability in air temperature anomalies were observed in the southern (σ = 2.4°C), lake (σ = 1.5°C), foothill (σ = 2.6°C), northern regions (σ = 1.9°C) when compared with air temperature variance in the positive AD modes in summer. Despite larger variability in spring and summer air-temperature anomalies,

these tended to be dampened during the autumn (Figure 4d) when air temperature anomalies did not deviate significantly from the long-term average. Of note, during autumn, there was less variability among sites during the strong negative (median = 0.3 to −0.04°C; σ = 1.3–1.5°C) and strong positive modes of the AD (median = −0.4 to −0.7°C; σ = 1.3–2.2°C).

In summary, the AD was a source of intraseasonal variability of air temperature over the NWT during summer. Results indicate that summer AD modes elicited the strongest response in air temperature, predominantly across southern, lake, and foothill regions. The influence of AD on air temperatures began in spring, intensified during summer, and was dampened during autumn. A clear spatial and gradual latitudinal response was displayed in the dataset, given the less evident AD–temperature relations at the northern region.

3.4 | Positive and negative modes of the AD index and precipitation amount

The amount of precipitation that falls during positive and negative modes of the AD varied across the Taiga Plains (Figure 6 and Table 1). There were few observable variations (from average) in total seasonal precipitation during strongly positive and negative modes of the AD. For example, during positive mode, winter precipitation anomalies were less variable (σ = 14.8 mm) than during negative modes (σ = 19.8 mm) (Figure 6b). These observed patterns in winter precipitation were not statistically significant ($p > .05$). In spring, across all regions, median precipitation anomalies remained near the long-term average during both AD modes (Figure 6b). In summer, median precipitation anomalies in the southern (median = −15.3 mm), lake (median = −10.1 mm), and northern regions (median = −3.2 mm), during negative modes of the AD were often lower than the long-term average. Further, summer precipitation anomalies had slightly greater variance during the positive mode of the AD (σ = 39.3 mm) compared with the negative AD mode (σ = 32.0 mm) across all regions (Figure 6c). However, there was no significance difference between the positive and negative AD mode across regions. During autumn, the southern (median = −9.1 mm), foothill (median = −9.2 mm), and northern (median = −3.9 mm) region precipitation anomalies were less than the long-term mean in the positive AD mode. In the negative AD mode, southern (median = 3.4 mm) and lake (median = 6.3 mm) regions, precipitation anomalies tend to be above the long-term mean with little difference to

TABLE 1 *p*-values the Kruskal–Wallis test for AD events exceeding the ±0.5 AD index thresholds were examined to quantify whether the mean climate variables anomalies (air temperature, precipitation, and onset date of sustained snowmelt) were significantly different during these positive and negative AD modes

	Air temperature				Precipitation				
Location	**Winter**	**Spring**	**Summer**	**Fall**	**Winter**	**Spring**	**Summer**	**Fall**	**Snowmelt onset**
Tuktoyaktuk	0.43	0.30	0.42	0.43	0.26	0.10	0.27	0.32	0.14
Aklavik	0.79	0.29	0.25	0.53	0.58	0.43	0.27	0.87	0.91
Fort McPherson	0.79	0.36	0.30	0.64	0.62	0.32	0.22	0.21	0.66
Fort Good Hope	0.37	0.87	0.09	0.36	0.98	0.55	0.80	0.78	0.28
Norman Wells	0.71	0.69	**0.09**	0.94	0.54	0.30	0.63	0.61	**0.04**
Tulita	0.75	0.72	**0.03**	0.97	0.54	0.25	0.77	0.17	0.51
Wrigley	0.54	0.69	**0.00**	0.97	0.58	0.41	0.58	**0.05**	0.08
Fort Reliance	0.66	0.58	**0.01**	0.25	0.34	0.29	0.58	0.61	0.43
Yellowknife	0.98	0.48	**0.01**	0.24	0.58	0.61	0.53	0.69	**0.02**
Fort Simpson	0.51	0.48	**0.00**	0.94	0.93	0.38	0.77	0.12	0.32
Fort Providence	0.58	0.45	**0.00**	0.94	0.75	0.48	0.85	0.97	0.26
Fort Resolution	0.84	0.27	**0.00**	0.48	0.54	0.48	0.29	0.53	0.08
Scotty Creek	0.43	0.50	**0.00**	0.97	0.98	0.27	0.51	0.08	0.11
Hay River	0.54	0.27	**0.00**	0.72	0.79	0.81	0.61	0.78	**0.04**
Fort Liard	0.21	0.48	**0.03**	0.97	0.84	1.00	0.27	**0.03**	0.20

Note: For *p*-values ≤.05 (bold) the null hypothesis is rejected, that is, there is no change in the mean climate variables anomaly during the positive and negative of AD mode.

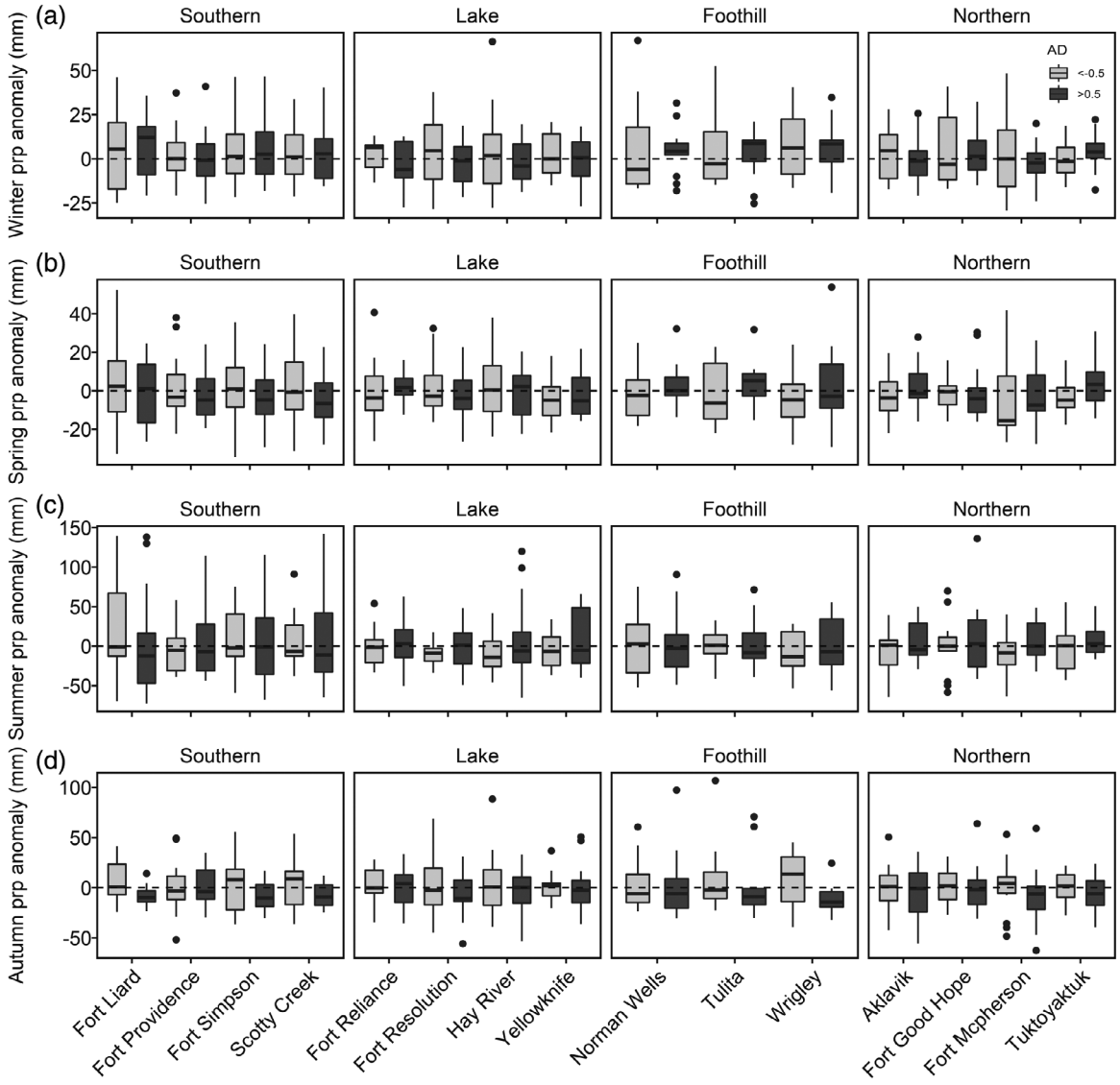

FIGURE 6 Boxplots displaying precipitation anomalies during positive (black boxes) and negative (grey boxes) modes of the AD index in winter, spring, summer, and fall. Anomalies are departures from 1950 to 2015 seasonal total precipitation. A positive anomaly indicates the observed precipitation was greater than the long-term total average while a negative anomaly indicates the observed precipitation was less than the long-term average. Black dots represent outliers

total seasonal precipitation in northern (median = 1.5 mm) and foothill regions (median = 1.6 mm) (Figure 6d). There were no significance differences ($p > .05$) in the distribution of precipitation anomalies during the two AD modes in autumn across the Taiga Plains. Although no distinct and persistent relations could be detected between strong AD modes and precipitation, statistical significance responses were dependent on specific locations and seasons. For instance, in autumn, Fort Liard (in southern region) Wrigley (in foothill region) experience significant difference in total seasonal precipitation during positive and negative modes of AD (Table 1).

3.5 | Positive and negative modes of the AD index and onset of snowmelt

Comparison between modes of AD and onset of snowmelt reveals consistent patterns across southern, lake, and foothill regions (Figure 7). Earlier onset of snowmelt occurred during years that also had positive mode of the AD in spring. In comparison, delays of snowmelt onset date for southern, lake, and foothills sites tended to occur during the negative mode of the AD (Figure 7). Further, all regions except farthest north (northern region) had greater variability in the timing of onset of snowmelt ($\sigma \sim$ 10–13 days; 6 days at northern sites) during the

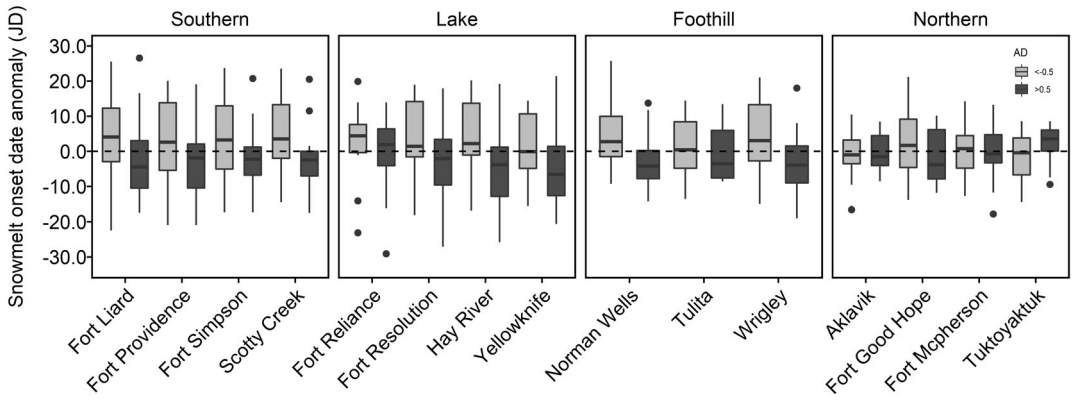

FIGURE 7 Deviation in the timing of snowmelt (in days) from the mean date of snowmelt during spring AD modes exceeding an index threshold of ±0.5. Black boxes represent positive AD mode and grey boxes represent negative AD mode. Black dots represent outliers. Positive anomaly on *y*-axis = later snowmelt; negative anomaly on *y*-axis = earlier snowmelt

negative mode of the AD. During the positive mode of the AD, there was a southern latitudinal shift towards progressively earlier onset dates of snowmelt, by an average of 3–5 days. The greatest difference in variability in onset snowmelt date occurred in southern (σ = 10 days) and lake sites (σ = 11 days), when compared with foothills (σ = 8 days) and northern sites (σ = 6 days). Despite the variability, snowmelt onset was significant ($p < .05$) at some foothills and lake sites, specifically Norman Wells, Yellowknife, and Hay River (Table 1).

4 | DISCUSSION

The results of this study indicate that when compared with long-term averages, greater magnitudes and higher summer air temperature anomalies occur during positive modes of the AD in southern, foothills, and lake sites (Figure 4). Air temperatures anomalies during positive modes of the AD tended to be greatest at southern sites, becoming more similar to the long-term average (less significantly different) with increasing latitude. Earlier onset of snowmelt by at least 5–11 days in the spring seasons also occurred during positive modes of the AD (Figure 7). Results indicate significant differences between snowmelt onset in spring and mean air temperatures in summer. However, there were no significantly large deviations in air temperature in winter during positive and negative modes of the AD. Further, there were no significant variations in total precipitation from the median during any of the seasons or regions studied. The results suggest that the variability of AD index values may be increasing in latter years (Figure 3). These results are consistent with Cai *et al.* (2018), who utilized ERA-Interim and CMIP5 model across the Arctic during the summer season between 1979 and 2016. They found that positive AD impacts summer air temperatures, while the influence of AD on total precipitation varied depending on the location (Cai *et al.*, 2018). These results noted for NWT also elicit the following questions: How do pressure differentials during the AD enhance positive temperature anomalies and changes in snowmelt onset? Why are precipitation anomalies during the AD difficult to discern or are nonexistent? Should we expect a warmer, possibly drier climate associated with increasing periodicity of the AD? This discussion will explore answers to some of these questions and will also provide insights on the implications of the AD on NWT terrestrial ecosystem climate.

4.1 | Mechanistic interactions between the AD and climate in the Taiga Plains

Inter- and intra-annual surface climate variability across Arctic and sub-Arctic regions may be explained by numerous atmospheric phenomena observed in the literature and described here. For example, the location, magnitude, and persistence of ridges and troughs influence weather and climate in northwestern Canada (Skinner *et al.*, 1999). During normal conditions, summer climate tends to be relatively dry in northwestern Canada (Skinner *et al.*, 1999). Occasionally, stagnant or slow moving ridges over western North America lead to warmer and drier conditions (Skinner *et al.*, 1999). Increased geopotential heights and ridging may be associated with the positive mode of the AD and results in sustained high pressure, reduced cloud cover and enhanced shortwave radiation receipt, and atmospheric warming (e.g., Figure 4) (Newton *et al.*, 2014; Bezeau *et al.*, 2015; Fazel-Rastgar, 2020). During the summers of 2000–2012, warm surface air anomalies were also observed over the Arctic Ocean, which were likely driven by meridional

movement of warm air masses from the south (Wang *et al.*, 2009; Overland *et al.*, 2012). In addition to and associated with these anomalies, Lackmann and Gyakum (1996) also noted elevated moisture transport to mid-level atmospheric layers (500, 700, and 800 mb) from the northern Pacific Ocean, thereby modulating weather and climate across the Taiga Plains by increasing the precipitation over the region. With regards to springtime onset of snowmelt (Figure 7), which is also related to warmer than average air temperatures, a recent study by Horvath *et al.* (2021) reported that the timing of melt onset in the Arctic was strongly influenced by atmospheric circulation patterns. Horvath *et al.* (2021) showed that prevailing pressure patterns associated with early melt onset in the Arctic were initiated by low SLP over Eurasia and high SLP over the Canadian Arctic Archipelago. This study noted similar pattern with SLP, and it is hypothesized that the onset of snowmelt in NWT (Figure 7) could have also been triggered or delayed by dipole circulation pattern prevalent during AD modes, but this requires additional investigation. During autumn at Wrigley and Fort Laird, there were some notable differences in precipitation during the strong positive and negative modes of AD, but these relations did not persist across all regions. The lack of a significant relationship between the AD and precipitation patterns could be because precipitation was likely influenced by local factors including topography, latitude, and proximity to landforms such as large lakes and mountains (Phillips, 1990). Thus, it may be more difficult to identify correspondence with synoptic-scale precipitation patterns and large-scale teleconnection anomalies.

Another hypothesis that may be responsible for mechanistic relations between the AD and air temperature (Figure 4) in NWT may be associated with the sea ice–albedo feedback (Watanabe *et al.*, 2006; Wang *et al.*, 2009; Tang *et al.*, 2014; Choi *et al.*, 2019; Xiao *et al.*, 2020). Sea ice modulates the connection between the atmosphere and the ocean by influencing heat and moisture exchanges at the air–sea interface (Watanabe *et al.*, 2006; Wang *et al.*, 2009; Tang *et al.*, 2014; Francis and Vavrus, 2015; Xiao *et al.*, 2020). As sea-ice extent decreases, surface albedo also decreases; thus, there is more open water and absorption of solar radiation increases, thereby accelerating warming (Serreze and Barry, 2014; Bezeau *et al.*, 2015; Lei *et al.*, 2016). Arctic sea ice has been declining since the 1980s, with amplification of these trends especially during the past decade (Wang *et al.*, 2009; Overland *et al.*, 2012). It has been suggested that the decline of Arctic sea ice has become sufficient to have a noticeable impact on large-scale atmospheric circulation (Zhang *et al.*, 2008; Overland and Wang, 2010; Serreze *et al.*, 2016). The negative AD has resulted in enhanced sea ice melt in the Arctic (Overland *et al.*, 2012; Choi *et al.*, 2019; Heo *et al.*, 2021). Lei *et al.* (2016) and Choi *et al.* (2019) found that positive SLP anomalies in most of the Arctic Basin and negative SLP anomalies over the northern Siberia/Barents Sea (Figure 2a) were associated with strong southerly winds from the northern Pacific, which bring in relatively warm air masses. These warm air masses enhance oceanic heat flux into the Arctic Ocean and results in increased sea ice melt, thereby further amplifying the ice–albedo feedback (Lei *et al.*, 2016; Choi *et al.*, 2019). Also, reduced sea ice is coincident with negative zonal wind anomalies at high latitudes, along with increased meridional flow in upper atmospheric layers (Tang *et al.*, 2014; Francis and Vavrus, 2015). These effects may lead to an enhanced meridional gradient in near-surface air temperature, resulting in the movement of air masses from southern to northern latitudes (Wang *et al.*, 2009; Overland *et al.*, 2012; Lei *et al.*, 2016). Warmer open water in the Arctic Ocean also warms the overlying atmosphere (Lei *et al.*, 2016; Heo *et al.*, 2021). Similarly, Overland *et al.* (2012) postulated that sea ice decline may have resulted in positive feedback associated with the movement of warmer air masses into the Arctic from the south. This movement of warmer air masses may have contributed to warmer than long-term average air temperature and earlier onset of snowmelt during the positive modes of the AD in spring in the NWT (Figure 5).

4.2 | Implications of AD and surface climate variability on terrestrial ecosystem in the Taiga Plains

The CMIP5 climate model predicts that the impacts of the AD in the Arctic will be enhanced during the 2006–2100 period, with higher-than-average air temperature and greater variability in cumulative precipitation during summer (Cai *et al.*, 2018). Increases in air temperature is known to induce permafrost thaw via a warmer ground and energy exchange at the surface, which has had significant impacts on changing water resources and terrestrial ecosystems in NWT (Wright *et al.*, 2009; Quinton *et al.*, 2011; Connon *et al.*, 2015; DeBeer *et al.*, 2016). Changes in surface climate variables alter local energy balance and changes albedo, which could exacerbate or reduce snowmelt in NWT (Chapin *et al.*, 2005; Helbig *et al.*, 2017). A shortened snow-covered season (Serreze and Barry, 2014; Chasmer and Hopkinson, 2017) and early snowmelt leads to exposure of the ground surface and litter to atmospheric warming and drying, which not only enhances permafrost thaw, but also increases the availability of fuels for wildland fire (Westerling, 2016), especially as depth to frost table increases (Sniderhan and

Baltzer, 2016). For example, the severe wildland fire year in 2014, when the largest areas burned occurred (Kochtubajda *et al.*, 2019), also corresponds with strong negative AD mode in spring and summer which was preceded by a strong positive AD mode during winter periods. With earlier snowmelt onset, there is also increased energy available for photosynthesis, lengthening of the growing season period (Lafleur and Humphreys, 2008; IPCC, 2021), and enhanced shrub growth (Chapin *et al.*, 2005; Baltzer *et al.*, 2014; Wilcox *et al.*, 2019). It is expected that shrubification in Arctic tundra regions and southern NWT may be amplified (Chasmer and Hopkinson, 2017; Mekonnen *et al.*, 2021). Bhatt *et al.* (2021) also illustrated that summer positive AD circulation, higher SLP over the Canadian Archipelago (defined as negative AD in this study) can influence local climate, which can have competing effects during the same AD mode on Arctic tundra vegetation across scales. For example, in the pan Arctic during the positive AD circulation in summer, open water in the Kara–Barents Seas was linked with below the long-term average vegetation greenness, indicated by maximum Normalized Difference Vegetation Index (MaxNDVI), and above the long-term average summer precipitation amounts between 1982 and 2019. However, the same positive AD circulation system in the Laptev Sea corresponded with above the long-term average vegetation greenness (MaxNDVI), total summer precipitation amounts, and summer warmth index on adjacent lands (Bhatt *et al.*, 2021). The present study found that the positive mode of the AD in spring resulted in earlier onset of snowmelt, while the opposite occurred during negative modes of the AD, especially in southern, lake, and foothill regions (Figure 7). Thus, the results observed here, across the NWT during positive AD, may be associated with amplified land-cover changes during AD circulation (Figure 4).

We hypothesize that the ridging pattern that is associated with the AD (Figure 4) could have also been a potential precursor to dry conditions and terrestrial ecosystem changes observed in NWT. For example, several studies have examined the influence of mid-atmospheric circulation to the presence of an anomalously strong ridge with coincident periods of warm and dry conditions, and the potential for increased severity and intensity of wildland fire in Canada (Skinner *et al.*, 1999; 2002; Serreze and Barry, 2014; Kochtubajda *et al.*, 2019; Jain and Flannigan, 2021). The presence of these strong ridges over the NWT may be related to positive AD modes. Increased tundra fires across the North Slope of Alaska, summer 2007, were attributed to the presence of a high-pressure circulation pattern over the Beaufort Sea (Alexeev *et al.*, 2015), a feature typical of the negative mode of the AD (Figure 2a). The atmospheric circulation linked negative AD modes may modulate the location and magnitude of ridges in the troposphere over the NWT, enhancing wildland fire in southern sites through the presence of an amplified ridge. For instance, the summer 2014 wildfire was attributed to the presence of slow moving ridges across the Canadian north in the NWT (Kochtubajda *et al.*, 2019). At the same time, the AD was in its negative mode (Figure 3). Additionally, wildland fires enable climate warming by accelerating active layer deepening and talik expansion in the boreal region (Gibson *et al.*, 2018). The latitudinal effect on the proportion of thaw in permafrost peatland (Gibson *et al.*, 2021), along with a coincident strong positive AD mode which elicited warmer temperature, also is indicative of the potential for continued widespread and amplified thawing throughout the discontinuous permafrost zone in western Canada. Permafrost thaw can also have significant implications for climate change over broad areas associated with increased microbial decomposition of unfrozen organic material and enhanced greenhouse gas emissions to the atmosphere (Turetsky *et al.*, 2007). Warming of soils and permafrost thaw stimulate microbial activity and decomposition of organic materials, thereby increasing respiration, carbon dioxide, and methane production (Helbig *et al.*, 2017).

4.3 | Recommendations for future study

The analysis presented here lays the groundwork for hypotheses on AD influences on local meteorology and the hydro-ecology of changing ecosystems in the NWT. However, an implicit assumption is the presence of a contemporaneous relationship between AD modes and surface climate variables. Here, it is assumed that atmospheric circulations associated with both AD modes operate independently to impact surface climate in the NWT. In some years this may not necessarily be a valid assumption since a lag/lead relationship between AD and surface climate variables are possible. This lag/lead linkage between atmospheric anomalies and impacts on local meteorology/climate is not uncommon for other teleconnections (e.g., El Niño–Southern Oscillation) across various regions (Shabbar *et al.*, 1997; McCabe and Dettinger, 1999). This study also acknowledges that teleconnections are not always independent, and feedbacks on climatology and weather patterns found in the NWT may be due to nonlinear, positive and negative teleconnection pattern interactions (Jiang *et al.*, 2014; Heo *et al.*, 2021). The effects of coupled teleconnections (e.g., AO and AD) on NWT hydroclimate will also require investigation. Although this research offered some insights into potential linkages between AD and surface climate for the NWT, additional research into the

robustness of some of the physical mechanisms explored here should be further investigated. This is important as future climate AD is predicted to drive greater variability of temperature and precipitation (Cai *et al*., 2018). For example, literature (e.g., Alexeev *et al*., 2015; Déry *et al*., 2009) indicates that drivers could exist between AD, hydroclimatology, and the potential for accelerated ecosystem changes observed in the Taiga Plains, but this requires further exploration. While these additional investigations are beyond scope of this research, the results of this analysis provides numerous avenues and hypotheses for improved understanding of the interactions between atmospheric teleconnection patterns, local meteorology, and ecosystem change.

5 | CONCLUSION

This study explored the relationship of strong positive and negative AD modes on seasonal air temperature, precipitation, and snowmelt onset anomalies in the Taiga Plains, NWT (Canada), during the past 66 years (1950–2015). The three main findings were (a) local air temperature increased during strong AD modes, which is intensified from southern, lake, foothill regions and to the northern regions of the Taiga Plains during summer; (b) local surface air temperature responses to AD were evident, but the coincident impact of AD on local cumulative precipitation were not; and (c) when AD is in its positive (negative) strong mode, earlier (later) onset date of snowmelt is observed when compared with the long-term average for southern, lake, and foothill regions and is more extreme in the southern and lakes regions. These results suggest that the strong AD modes could be a precursor for certain characteristic mid- to upper-level geopotential heights/pressure patterns and surface climate responses, which has implications for rapidly changing ecosystems in the NWT especially across southern regions which have more sensitive patches of ecosystem (Rouse *et al*., 1997). The air temperature/snowmelt onset north–south response to the AD maybe linked to the position and intensity of the geopotential heights ridge axis over the NWT and sea-ice feedback as previous studies identified similar characteristic mid- to upper-level geopotential heights/pressure patterns known to persist in the northwestern Canada (e.g., Kochtubajda *et al*., 2019). This requires further exploration.

Although there is much to learn about the interactions between a rapidly warming NWT and large-scale teleconnection patterns, this study identified notable association between surface climate variables and strong AD modes. This has direct relevance to NWT communities, especially as these communities are among the most vulnerable in Canada to climate-induced environmental change. This study also implies that if a developing strong AD mode were to be detected early enough, threats like heatwaves and wildland fires, as well as their ecological consequences, could be better anticipated, hence enabling northern governments to be better prepared for wildland fire seasons. This work also provides insights for hydrometeorological modellers in their efforts to improve weather and climate models. Furthermore, NWT population that resides in the Taiga Plains will also benefit as these findings may help strengthen climate adaptation and mitigation polices in the NWT at the local level.

AUTHOR CONTRIBUTIONS

Conceptualization: B. D. Persaud, L. E. Chasmer, M. C. English, W. L. Quinton, and B. B. Wolfe. *Data curation and formal analysis*: B. D. Persaud. *Funding acquisition*: W. L. Quinton. *Methodology*: B. D. Persaud and L. E. Chasmer. Supervision: L. E. Chasmer, W. L. Quinton, B. B. Wolfe, and M. C. English. *Writing – original draft*: B. D. Persaud. *Writing – review and editing*: B. D. Persaud, L. E. Chasmer, B. B. Wolfe, M. C. English, and W. L. Quinton.

ACKNOWLEDGEMENTS

We thank Natural Resources Canada, especially Drs. Daniel McKenny and Pia Papadopol, for making available ANUSPLIN daily temperature and precipitation data. Thanks to Julie Grant for her help with the figures. Funds for this work were partially provided by Wilfrid Laurier University and ArcticNet Programme. The analyses were performed using research facilities made available via the Canada First Research Excellence Fund's Global Water Futures Programme. We also thank the two anonymous reviewers and editors for their helpful insights and suggestions that contributed towards the final version of manuscript.

DATA AVAILABILITY STATEMENT

The Arctic Dipole index data were downloaded from the United States National Oceanic and Atmospheric Administration https://www.beringclimate.noaa.gov/data/. ANUSPLIN daily temperature and precipitation data for Canada were provided by Natural Resources Canada staff via this link ftp://ftp.nrcan.gc.ca/pub/outgoing/canada_daily_grids data last accessed in 2019.

ORCID

Bhaleka D. Persaud https://orcid.org/0000-0003-2785-3954
Laura E. Chasmer https://orcid.org/0000-0002-8062-1530
William L. Quinton https://orcid.org/0000-0001-5707-4519
Brent B. Wolfe https://orcid.org/0000-0003-4093-453X

REFERENCES

Alexeev, V.A., Euskirchen, E.S., Cherry, J.E. and Busey, R.C. (2015) Tundra burning in 2007—Did sea ice retreat matter? *Polar Science*, 9(2), 185–195. https://doi.org/10.1016/j.polar.2015.02.002.

Baltzer, J.L., Veness, T., Chasmer, L.E., Sniderhan, A.E. and Quinton, W.L. (2014) Forests on thawing permafrost: fragmentation, edge effects, and net forest loss. *Global Change Biology*, 20(3), 824–834.

Barnston, A.G. and Livezey, R.E. (1987) Classification, seasonality and persistence of low-frequency atmospheric circulation patterns. *Monthly Weather Review*, 115(6), 1083–1126. https://doi.org/10.1175/1520-0493(1987)1152.0.CO;2.

Bezeau, P., Sharp, M. and Gascon, G. (2015) Variability in summer anticyclonic circulation over the Canadian Arctic Archipelago and West Greenland in the late 20th/early 21st centuries and its effect on glacier mass balance. *International Journal of Climatology*, 35(4), 540–557. https://doi.org/10.1002/joc.4000.

Bhatt, U.S., Walker, D.A., Raynolds, M.K., Walsh, J.E., Bieniek, P. A., Cai, L., Comiso, J.C., Epstein, H.E., Frost, G.V., Gersten, R. and Hendricks, A.S. (2021) Climate drivers of Arctic tundra-variability and change using an indicators framework. *EnvironmentalResearchLetters*, 16(5), 055019. https://doi.org/10.1088/1748-9326/abe676.

Bonsal, B. and Shabbar, A. (2011) *Large-scale climate oscillations influencing Canada, 1900–2008. Canadian biodiversity: ecosystem status and trends 2010*. Ottawa, ON: Canadian Councils of Resource Ministers. Technical thematic report no. 4. Available at: http://www.biodivcanada.ca/default.asp?lang=En&n=137E1147-0.

Budikova, D. (2009). Role of Arctic sea ice in global atmospheric circulation: A review. *Global and Planetary Change*, 68(3), 149-163. https://doi.org/10.1016/j.gloplacha.2009.04.001

Cai, L., Alexeev, V.A., Walsh, J.E. and Bhatt, U.S. (2018) Patterns, impacts, and future projections of summer variability in the Arctic from CMIP5 models. *Journal of Climate*, 31(24), 9815–9833. https://doi.org/10.1175/JCLI-D-18-0119.1.

Chapin III, F.S., Sturm, M., Serreze, M.C., McFadden, J.P., Key, J. R., Lloyd, A.H., McGuire, A.D., Rupp, T.S., Lynch, A.H., Schimel, J.P. and Beringer, J. (2005) Role of land-surface changes in Arctic summer warming. *Science*, 310(5748), 657–660. https://www.science.org/doi/10.1126/science.1117368.

Chasmer, L. and Hopkinson, C. (2017) Threshold loss of discontinuous permafrost and landscape evolution. *Global Change Biology*, 23(7), 2672–2686. https://doi.org/10.1111/gcb.13537.

Choi, N., Kim, K., Lim, Y. and Lee, M. (2019) Decadal changes in the leading patterns of sea level pressure in the Arctic and their impacts on the sea ice variability in boreal summer. *Cryosphere*, 13(11), 3007–3021. https://doi.org/10.5194/tc-13-3007-2019.

Connon, R.F., Chasmer, L., Haughton, E., Helbig, M., Hopkinson, C., Sonnentag, O. and Quinton, W.L. (2021) The implications of permafrost thaw and land cover change on snow water equivalent accumulation, melt and runoff in discontinuous permafrost peatlands. *Hydrological Processes*, 35(9), e14363. https://doi.org/10.1002/hyp.14363.

Connon, R.F., Quinton, W.L., Craig, J.R., Hanisch, J. and Sonnentag, O. (2015) The hydrology of interconnected bog complexes in discontinuous permafrost terrains. *Hydrological Processes*, 29(18), 3831–3847. https://doi.org/10.1002/hyp.10604.

DeBeer, C.M., Wheater, H.S., Carey, S.K. and Chun, K.P. (2016) Recent climatic, cryospheric, and hydrological changes over the interior of western Canada: a review and synthesis. *Hydrology and Earth System Sciences*, 20(4), 1573–1598. https://doi.org/10.5194/hess-20-1573-2016.

Déry, S.J., Hernández-Henríquez, M.A., Burford, J.E. and Wood, E. F. (2009) Observational evidence of an intensifying hydrological cycle in northern Canada. *Geophysical Research Letters*, 36(13), L13402.

Déry, S.J. and Wood, E.F. (2004) Teleconnection between the Arctic Oscillation and Hudson Bay river discharge. *Geophysical Research Letters*, 31(18), L18205. https://doi.org/10.1029/2004GL020729.

Dyke, L.D. and Brooks, G.R. (2000) *The Physical Environment of the Mackenzie Valley, Northwest Territories: A Base Line for the Assessment of Environmental Change*. Ottawa, ON: Geological Survey of Canada.

Ecosystem Classification Group. (2009) *Ecological regions of the Northwest Territories, Taiga Plains*. Yellowknife, NT: Department of Environment and Natural Resources, Government of the Northwest. Available at: https://www.enr.gov.nt.ca/sites/enr/files/resources/taiga_plains_ecological_land_classification_report.pdf.

Fazel-Rastgar, F. (2020) Synoptic climatological approach associated with three recent summer heatwaves in the Canadian Arctic. *Journal of Water and Climate Change*, 11(S1), 233–250. https://doi.org/10.2166/wcc.2020.281.

Fleming, S.W., Moore, R.D. and Clarke, K.C. (2006) Glacier-mediated streamflow teleconnections to the Arctic Oscillation. *International Journal of Climatology*, 26(5), 619–636. https://doi.org/10.1002/joc.1273.

Francis, J.A. and Vavrus, S.J. (2015) Evidence for a wavier jet stream in response to rapid Arctic warming. *Environmental Research Letters*, 10(1), 014005. https://doi.org/10.1088/1748-9326/10/1/014005.

Gibson, C., Cottenie, K., Gingras-Hill, T., Kokelj, S.V., Baltzer, J.L., Chasmer, L. and Turetsky, M.R. (2021) Mapping and understanding the vulnerability of northern peatlands to permafrost thaw at scales relevant to community adaptation planning. *Environmental Research Letters*, 16(5), 055022. https://doi.org/10.1088/1748-9326/abe74b.

Gibson, C.M., Chasmer, L.E., Thompson, D.K., Quinton, W.L., Flannigan, M.D. and Olefeldt, D. (2018) Wildfire as a major driver of recent permafrost thaw in boreal peatlands. *Nature Communications*, 9(1), 3041. https://doi.org/10.1038/s41467-018-05457-1.

Helbig, M., Chasmer, L.E., Kljun, N., Quinton, W.L., Treat, C.C. and Sonnentag, O. (2017) The positive net radiative greenhouse gas forcing of increasing methane emissions from a thawing boreal forest-wetland landscape. *Global Change Biology*, 23(6), 2413–2427. https://doi.org/10.1111/gcb.13520.

Helsel, D.R. and Hirsch, R.M. (1992) *Statistical Methods in Water Resources*. Amsterdam: Elsevier.

Heo, E., Sung, M., An, S. and Yang, Y. (2021) Decadal phase shift of summertime Arctic Dipole pattern and its nonlinear effect on sea ice extent. *International Journal of Climatology*, 41(9), 4732–4742. https://doi.org/10.1002/joc.7097.

Horvath, S., Stroeve, J., Rajagopalan, B. and Jahn, A. (2021) Arctic sea ice melt onset favored by an atmospheric pressure pattern reminiscent of the north American Eurasian Arctic pattern. *Climate Dynamics*, 57(7), 1771–1787. https://doi.org/10.1007/s00382-021-05776-y.

Hutchinson, M.F., Mckenny, D.W., Lawrence, K., Pedlar, J.H., Hopkinson, R.F., Mileweska, E. and Papadpol, P. (2009) Development and testing of Canada-wide interpolated spatial models of daily minimum–maximum temperature and precipitation for 1961–2003. *Journal of Applied Meteorology and Climatology*, 48(4), 725–741. https://doi.org/10.1175/2008JAMC1979.1.

IPCC. (2021) In: Masson-Delmotte, V., Zhai, P., Pirani, A., Connors, S.L., Péan, C., Berger, S., Caud, N., Chen, Y., Goldfarb, L., Gomis, M.I., Huang, M., Leitzell, K., Lonnoy, E., Matthews, J.B.R., Maycock, T.K., Waterfield, T., Yelekçi, O., Yu, R. and Zhou, B. (Eds.) *Climate Change 2021: The Physical Science Basis. Contribution of Working Group I to the Sixth Assessment Report of the Intergovernmental Panel on Climate Change*. Cambridge: Cambridge University Press.

Jain, P. and Flannigan, M. (2021) The relationship between the polar jet stream and extreme wildfire events in North America. *Journal of Climate*, 34(15), 6247–6265. https://doi.org/10.1175/JCLI-D-20-0863.1.

Jiang, R., Gan, T.Y., Xie, J. and Wang, N. (2014) Spatiotemporal variability of Alberta's seasonal precipitation, their teleconnection with large-scale climate anomalies and sea surface temperature. *International Journal of Climatology*, 34(9), 2899–2917. https://doi.org/10.1002/joc.3883.

Kalnay, E., Kanamitsu, M., Kistler, R., Collins, W., Deaven, D., Gandin, L. and Woollen, J. (1996) The NCEP/NCAR 40-year reanalysis project. *Bulletin of the American Meteorological Society*, 77(3), 437–472.

Kochtubajda, B., Stewart, R.E., Flannigan, M.D., Bonsal, B.R., Cuell, C. and Mooney, C.J. (2019) An assessment of surface and atmospheric conditions associated with the extreme 2014 wildfire season in Canada's Northwest Territories. *Atmosphere-Ocean*, 57(1), 73–90. https://doi.org/10.1080/07055900.2019.1576023.

Lackmann, G.M. and Gyakum, J.R. (1996) The synoptic- and planetary-scale signatures of precipitating systems over the Mackenzie River basin. *Atmosphere-Ocean*, 34(4), 647–674. https://doi.org/10.1080/07055900.1996.9649581.

Lafleur, P.M. and Humphreys, E.R. (2008) Spring warming and carbon dioxide exchange over low Arctic tundra in central Canada. *Global Change Biology*, 14(4), 740–756.

Lei, R., Tian-Kunze, X., Leppäranta, M., Wang, J., Kaleschke, L. and Zhang, Z. (2016) Changes in summer sea ice, albedo, and portioning of surface solar radiation in the Pacific sector of Arctic Ocean during 1982–2009. *Journal of Geophysical Research: Oceans*, 121(8), 5470–5486.

Matsumura, S., Zhang, X. and Yamazaki, K. (2014) Summer Arctic atmospheric circulation response to spring Eurasian snow cover and its possible linkage to accelerated sea ice decrease. *Journal of Climate*, 27(17), 6551–6558. https://doi.org/10.1175/JCLI-D-13-00549.1.

McCabe, G.J. and Dettinger, M.D. (1999) Decadal variations in the strength of ENSO teleconnections with precipitation in the western United States. *International Journal of Climatology*, 19(13), 1399–1410. https://doi.org/10.1002/(SICI)1097-0088(19991115)19:133.0.CO;2-A.

McKenney, D.W., Hutchinson, M.F., Papadopol, P., Lawrence, K., Pedlar, J., Campbell, K. and Owen, T. (2011) Customized spatial climate models for North America. *Bulletin of the American Meteorological Society*, 92(12), 1611–1622. https://doi.org/10.1175/2011BAMS3132.1.

Mekonnen, Z.A., Riley, W.J., Berner, L.T., Bouskill, N.J., Torn, M.S., Iwahana, G., Breen, A.L., Myers-Smith, I.H., Criado, M.G., Liu, Y. and Euskirchen, E.S. (2021) Arctic tundra shrubification: a review of mechanisms and impacts on ecosystem carbon balance. *Environmental Research Letters*, 16(5), 053001. https://doi.org/10.1088/1748-9326/abf28b.

Newton, B.W., Prowse, T.D. and Bonsal, B.R. (2014) Evaluating the distribution of water resources in western Canada using synoptic climatology and selected teleconnections. Part 2: summer season. *Hydrological Processes*, 28(14), 4235–4249. https://doi.org/10.1002/hyp.10235.

NOAA. (2020) *NOAA Climate Analysis and Plotting tool*. Boulder, CO: NOAA PSL. Available at: https://psl.noaa.gov/cgi-bin/data/getpage.p [Accessed on 15th December 2020].

NOAA. (2021) *Bering climate*. Boulder, CO: NOAA. Available at: https://www.beringclimate.noaa.gov/data/index.php [Accessed on 15th August 2021].

NRCAN. (2019) *Natural resources Canada ANUSPLIN data*. Available at: ftp://ftp.nrcan.gc.ca/pub/outgoing/canada_daily_grids.

Overland, J.E., Francis, J.A., Hanna, E. and Wang, M. (2012) The recent shift in early summer Arctic atmospheric circulation. *Geophysical Research Letters*, 39(19), L19804. https://doi.org/10.1029/2012GL053268.

Overland, J.E. and Wang, M. (2010) Large-scale atmospheric circulation changes are associated with the recent loss of Arctic Sea ice. *Tellus, Series A: Dynamic Meteorology and Oceanography*, 62(1), 1–9. https://doi.org/10.1111/j.1600-0870.2009.00421.x.

Persaud, B.D., Whitfield, P.H., Quinton, W.L. and Stone, L.E. (2020) Evaluating the suitability of three gridded-datasets and their impacts on hydrological simulation at Scotty Creek in the southern Northwest Territories, Canada. *Hydrological Processes*, 34(4), 898–913. https://doi.org/10.1002/hyp.13663.

Phillips, D. (1990) *The climates of Canada*. Ottawa, ON: Ministry of Supply and Services Canada. Catalogue no. En56-1/1990E, 176 pp.

Quinton, W.L., Hayashi, M. and Chasmer, L.E. (2011) Permafrost-thaw-induced land-cover change in the Canadian subarctic: implications for water resources. *Hydrological Processes*, 25(1), 152–158. https://doi.org/10.1002/hyp.7894.

R Development Core Team. (2016) *R: a language and environment for statistical computing*. Vienna: R Foundation for Statistical Computing. Available at: https://www.R-project.org/.

Rouse, W.R., Douglas, M.S., Hecky, R.E., Hershey, A.E., Kling, G.W., Lesack, L., Marsh, P., McDonald, M., Nicholson, B.J., Roulet, N.T. and Smol, J.P. (1997) Effects of climate change on the freshwaters of Arctic and Subarctic North America. *Hydrological Processes*, 11(8), 873–902. https://doi.org/10.1002/(SICI)1099-1085(19970630)11:8<873::AID-HYP510>3.0.CO;2-6.

Serreze, M.C. and Barry, R.G. (2014) *The Arctic Climate System*. New York, NY: Cambridge University Press.

Serreze, M.C., Stroeve, J., Barrett, A.P. and Boisvert, L.N. (2016) Summer atmospheric circulation anomalies over the Arctic Ocean and their influences on September Sea ice extent: a cautionary tale. *Journal of Geophysical Research: Atmospheres*, 121(19), 11463–11485. https://doi.org/10.1002/2016JD025161.

Shabbar, A., Bonsal, B. and Khandekar, M. (1997) Canadian precipitation patterns associated with the Southern Oscillation. *Journal of Climate*, 10(12), 3016–3027. https://doi.org/10.1175/1520-0442(1997)0102.0.CO;2.

Shi, X., Marsh, P. and Yang, D. (2015) Warming spring air temperatures, but delayed spring streamflow in an Arctic headwater basin. *Environmental Research Letters*, 10(6), 64003. https://doi.org/10.1088/1748-9326/10/6/064003.

Skinner, W.R., Flannigan, M.D., Stocks, B.J., Martell, D.L., Wotton, B. M., Todd, J.B., Mason, J.A., Logan, K.A. and Bosch, E.M. (2002) A 500 hPa synoptic wildland fire climatology for large Canadian forest fires, 1959–1996. *Theoretical and Applied Climatology*, 71(3), 157–169. https://doi.org/10.1007/s007040200002.

Skinner, W.R., Stocks, B.J., Martell, D.L., Bonsal, B. and Shabbar, A. (1999) The association between circulation anomalies in the mid-troposphere and area burned by wildland fire in Canada. *Theoretical and Applied Climatology*, 63(1), 89–105.

Sniderhan, A.E. and Baltzer, J.L. (2016) Growth dynamics of black spruce (*Picea mariana*) in a rapidly thawing discontinuous permafrost peatland. *Journal of Geophysical Research: Biogeosciences*, 121(12), 2988–3000. https://doi.org/10.1002/2016JG003528.

Tan, X., Gan, T.Y., Chen, S. and Liu, B. (2019) Modeling distributional changes in winter precipitation of Canada using Bayesian spatiotemporal quantile regression subjected to different teleconnections. *Climate Dynamics*, 52(3), 2105–2124.

Tang, Q., Zhang, X. and Francis, J.A. (2014) Extreme summer weather in northern mid-latitudes linked to a vanishing cryosphere. *Nature Climate Change*, 4(1), 45–50.

Thompson, D.W. and Wallace, J.M. (1998) The Arctic Oscillation signature in the wintertime geopotential height and temperature fields. *Geophysical Research Letters*, 25(9), 1297–1300.

Trenberth, K.E. (1997) The definition of El Niño. *Bulletin of the American Meteorological Society*, 78(12), 2771–2778. https://doi.org/10.1175/1520-0477(1997)0782.0.CO;2.

Tukey, J.W. (1949) Comparing individual means in the analysis of variance. *Biometrics*, 5, 99–114.

Turetsky, M.R., Wieder, R.K., Vitt, D.H., Evans, R.J. and Scott, K.D. (2007) The disappearance of relict permafrost in boreal North America: effects on peatland carbon storage and fluxes. *Global Change Biology*, 13(9), 1922–1934.

Vincent, L.A., Zhang, X., Brown, R.D., Feng, Y., Mekis, E., Milewska, E.J., Wan, H. and Wang, X.L. (2015) Observed trends in Canada's climate and influence of low-frequency variability modes. *Journal of Climate*, 28(11), 4545–4560. https://doi.org/10.1175/JCLI-D-14-00697.1.

Wallace, J.M. and Gutzler, D.S. (1981) Teleconnections in the geopotential height field during the northern hemisphere winter. *Monthly Weather Review*, 109(4), 784–812.

Wang, J., Zhang, J., Watanabe, E., Ikeda, M., Mizobata, K., Walsh, J.E., Bai, X. and Wu, B. (2009) Is the dipole anomaly a major driver to record lows in Arctic summer sea ice extent? *Geophysical Research Letters*, 36(5), L05706. https://doi.org/10.1029/2008GL036706.

Watanabe, E., Wang, J., Sumi, A. and Hasumi, H. (2006) Arctic Dipole anomaly and its contribution to sea ice export from the Arctic Ocean in the 20th century. *Geophysical Research Letters*, 33(23), L23703. https://doi.org/10.1029/2006GL028112.

Westerling, A.L. (2016) Increasing western US forest wildfire activity: sensitivity to changes in the timing of spring. *Philosophical Transactions of the Royal Society of London. Series B, Biological Sciences*, 371(1696), 20150178. https://doi.org/10.1098/rstb.2015.0178.

Wilcox, E.J., Keim, D., de Jong, T., Walker, B., Sonnentag, O., Sniderhan, A.E., Mann, P. and Marsh, P. (2019) Tundra shrub expansion may amplify permafrost thaw by advancing snowmelt timing. *Arctic Science*, 5(4), 202–217. https://doi.org/10.1139/as-2018-0028.

Wong, J.S., Razavi, S., Bonsal, B.R., Wheater, H.S. and Asong, Z.E. (2017) Inter-comparison of daily precipitation products for large-scale hydro-climatic applications over Canada. *Hydrology and Earth System Sciences*, 21(4), 2163–2185. https://doi.org/10.5194/hess-21-2163-2017.

Woo, M., Rouse, W.R., Stewart, R.E. and Stone, J.M.R. (2008) *The Mackenzie GEWEX Study: A Contribution to Cold Region Atmospheric and Hydrologic Sciences*. Berlin-Heidelberg: Springer. https://doi.org/10.1007/978-3-540-73936-4_1.

Wright, N., Hayashi, M. and Quinton, W.L. (2009) Spatial and temporal variations in active layer thawing and their implication on runoff generation in peat-covered permafrost terrain. *Water Resources Research*, 45(5), W05414. https://doi.org/10.1029/2008WR006880.

Wu, B., Zhang, R., Wang, B. and D'Arrigo, R. (2009) On the association between spring Arctic sea ice concentration and Chinese summer rainfall. *Geophysical Research Letters*, 36(9), L09501. https://doi.org/10.1029/2009GL037299.

Wu, B., Zhang, R. and Wang, J. (2005) Dipole anomaly in the Arctic atmosphere and winter Arctic sea ice motion. *Science in China Series D, Earth Sciences*, 48(9), 1529–1536. https://doi.org/10.1360/04yd0174.

Xiao, K., Chen, M., Wang, Q., Wang, X. and Zhang, W. (2020) Low-frequency sea level variability and impact of recent sea ice decline on the sea level trend in the Arctic Ocean from a high-resolution simulation. *Ocean Dynamics*, 70(6), 787–802. https://doi.org/10.1007/s10236-020-01373-5.

Zhang, J., Lindsay, R., Steele, M. and Schweiger, A. (2008) What drove the dramatic retreat of Arctic Sea ice during summer 2007? *Geophysical Research Letters*, 35(11), L11505. https://doi.org/10.1029/2008GL034005.

How to cite this article: Persaud, B. D., Chasmer, L. E., Quinton, W. L., Wolfe, B. B., & English, M. C. (2022). Sensitivity of seasonal air temperature and precipitation, and onset of snowmelt, to Arctic Dipole modes across the Taiga Plains, Northwest Territories, Canada. *International Journal of Climatology*, 1–18. https://doi.org/10.1002/joc.7810